



# Passivation of defect states in anatase $\text{TiO}_2$ hollow spheres with Mg doping: Realizing efficient photocatalytic overall water splitting

Linjie Gao<sup>a</sup>, Yaguang Li<sup>a,\*</sup>, Jiaxin Ren<sup>b</sup>, Shufang Wang<sup>a</sup>, Ruining Wang<sup>a</sup>, Guangsheng Fu<sup>a,\*</sup>, Yong Hu<sup>b,\*</sup>

<sup>a</sup> Hebei Key Lab of Optic-Electronic Information and Materials, The College of Physics Science and Technology, Hebei University, Baoding, 071002, China

<sup>b</sup> Key Laboratory of the Ministry of Education for Advanced Catalysis Materials, Institute of Physical Chemistry, Zhejiang Normal University, Jinhua, 321004, China



## ARTICLE INFO

### Article history:

Received 12 July 2016

Received in revised form 13 August 2016

Accepted 6 September 2016

Available online 9 September 2016

### Keywords:

$\text{TiO}_2$

Hollow spheres

Defect states

Mg doping

Overall water splitting

## ABSTRACT

Since tremendous numbers of defect states are distributed in anatase  $\text{TiO}_2$  materials, the photocatalytic overall water splitting (POWS) can not be occurred on anatase  $\text{TiO}_2$  nanostructures under normal sunlight. Meanwhile, it is still lacking of effective method to suppress the intrinsic defect states in anatase  $\text{TiO}_2$ . In the present work, it has been found that the defect induced light absorption in anatase  $\text{TiO}_2$  hollow spheres could be reduced by Mg doping. In-depth detecting of the defect states evolution is investigated by the transient infrared absorption-excitation energy scanning spectroscopic measurement (TRIRA-EESS), indicating that the Mg doping could eliminate the intrinsic deep defect states and weaken the shallow defect states in  $\text{TiO}_2$ . The efficient and stable sunlight-driven POWS is firstly realized on anatase  $\text{TiO}_2$  hollow spheres only after doping of Mg rather than Ni, Cr. The  $\text{H}_2$  and  $\text{O}_2$  evolution rates can be as high as 850 and 425  $\mu\text{mol g}^{-1} \text{h}^{-1}$ , respectively. First principle calculations reveal that the weakening of defect states in Mg doped anatase  $\text{TiO}_2$  is mainly caused by the unique electronic structure of Mg dopant.

© 2016 Elsevier B.V. All rights reserved.

## 1. Introduction

Photocatalytic overall water splitting (POWS) for hydrogen generation is one of the most promising ways for supplying clean and sustainable energy [1–3]. Titanium dioxide ( $\text{TiO}_2$ ) is the benchmark semiconductor used in photocatalysis [4–6]. Among the three phases of  $\text{TiO}_2$ , anatase is the most active phase for photocatalytic  $\text{H}_2$  generation [7,8]. In recent decades, many groups have tried variety of methods, such as nanotechnology, selective facets, cocatalysts, etc., to modify the anatase  $\text{TiO}_2$  [9–11]. And there has been a great progress in photocatalytic half water splitting for  $\text{H}_2$  production [12,13]. However, defects are inevitably distributed in anatase  $\text{TiO}_2$  [14]. The defects could introduce tremendous numbers of defect states in the band gap, which always cause carriers' recombination [15,16]. More seriously, the defect states could weaken the photo-generated carriers' oxidation and reduction capacities in anatase  $\text{TiO}_2$  [17]. Li and Weng et al. found that large numbers of defect states especially the deep trapping states are lying in the band gap of anatase  $\text{TiO}_2$  [18], thereby impeding the POWS real-

ization on anatase  $\text{TiO}_2$  [19]. Consequently, the POWS has never been taken place on anatase  $\text{TiO}_2$  materials under normal sunlight, despite anatase  $\text{TiO}_2$  has a suitable band structure both for photocatalytic water reduction and oxidation [20,21]. Therefore, suppression of the defect states in anatase  $\text{TiO}_2$  is the key for further developing their applications in photocatalysis. Li et al. reported that a part of defect states in anatase  $\text{TiO}_2$  could be suppressed by ultrasensitive ultraviolet irradiation [19]. However, the defect states were only temporary suppressed and could be recovered without the irradiation of the specific light source. Reviewing the previous results, it is still lacking of efficient and stable method to reduce the defect states in anatase  $\text{TiO}_2$ .

To date, various transition metal elements have doped into the  $\text{TiO}_2$  lattice [22]. The electrons on d orbit have abundant energy levels, which could cause more interband states [23–25]. Thus, doping with transition metal elements in  $\text{TiO}_2$  is always introducing more considerable trapping states, which are widely considered to be harmful to the POWS realization [26,27]. However, Mg elements have not the complicated d orbit electrons and the ionic radius of  $\text{Mg}^{2+}$  (65 pm) is similar of  $\text{Ti}^{4+}$  (68 pm). For instance, Iwamoto and Hanaya have reported that Mg doping could promote the energy position of conduction band minimum, which is very different from the transition metal doping [28,29]. Herein, through the experiments

\* Corresponding authors.

E-mail addresses: [yaguang\\_1987@126.com](mailto:yaguang_1987@126.com) (Y. Li), [fugs@hbu.edu.cn](mailto:fugs@hbu.edu.cn) (G. Fu), [yonghu@zjnu.edu.cn](mailto:yonghu@zjnu.edu.cn) (Y. Hu).

and first principle calculations, we found that the Mg doping could suppress rather than introduce trapping states in anatase  $\text{TiO}_2$ . Therefore, the efficient and stable POWS under normal sunlight is achieved on the Mg doped anatase  $\text{TiO}_2$  ultrathin hollow spheres.

## 2. Experimental section

### 2.1. Materials synthesis

The carbon spheres were hydrothermally synthesized using the method reported by Sun et al. [30,31]. To synthesize the 0.5% Mg doped  $\text{TiO}_2$  ( $\text{Mg-TiO}_2$ ) ultrathin hollow spheres, 50 mg of as-prepared carbon spheres was dispersed in 100 mL anhydrous ethanol by ultrasonication, followed by adding 3 mg of  $\text{Mg}(\text{NO}_3)_2 \cdot 6\text{H}_2\text{O}$  and 1 g tetrabutyl titanate. The as-obtained mixture was stirred for 4 h. A rinsing process involving two cycles of centrifugation/washing/re-dispersion was performed with anhydrous ethanol. After dried in an oven in air at 80 °C for 6 h, the  $\text{Mg-TiO}_2$  ultrathin hollow spheres were obtained by calcinating the products in air at 400 °C for 12 h. The continuously variable concentration of Mg ions in  $\text{TiO}_2$  could be attempted by regulating the concentration of  $\text{Mg}(\text{NO}_3)_2 \cdot 6\text{H}_2\text{O}$  in the solution. The as-prepared catalyst for  $\text{H}_2$  production and POWS was modified with Pt as a cocatalyst for water splitting based on photo-deposition method reported elsewhere [32]. Briefly, a moderate amount of  $\text{H}_2\text{PtCl}_6$  was mixed in the aqueous (90%)/methanol (10%) solution containing samples. Then the solution was put under a 300 W xenon lamp. The synthesis of Ni, Cr doped anatase  $\text{TiO}_2$  hollow spheres is similar to that of  $\text{Mg-TiO}_2$  hollow spheres preparation except of changing the  $\text{Mg}(\text{NO}_3)_2 \cdot 6\text{H}_2\text{O}$  as  $\text{Ni}(\text{NO}_3)_2 \cdot 6\text{H}_2\text{O}$  and  $\text{Cr}(\text{NO}_3)_2 \cdot 9\text{H}_2\text{O}$  respectively. The rutile  $\text{TiO}_2$  sample is obtained by calcination of the P25 at 1000 °C for 12 h.

### 2.2. Materials characterization

Inductive coupled plasma and atomic absorption spectroscopy (ICP-AAS) measurements were used to analyze the ratio of Mg and Ti in samples, after digesting the  $\text{Mg-TiO}_2$  hollow spheres in hot sulfuric acid (4 M  $\text{H}_2\text{SO}_4$  solution). The Mg in 1% doped concentration was detected precisely by ICP-AAS, whereas, the Mg doping concentration in 0.1 and 0.5 was the averaged value of five independent ICP-AAS measurements. The structure properties of  $\text{Mg-TiO}_2$  hollow spheres were characterized by X-ray diffraction (XRD), field emission scanning electron microscopy (SEM) and high-resolution TEM (HR-TEM). The chemical states of samples were measured by X-ray photoelectron spectroscope (XPS). The Raman spectroscopy of all the samples was recorded on a Dilor Labram-1B microspectrometer. UV-vis diffuse reflectance experiments were carried out on an ultraviolet-visible spectrophotometer. To further investigate the thermodynamics for different POWS performances on  $\text{Mg-TiO}_2$  hollow sphere based photocatalysts, the midgap energy level of Mg-doped anatase  $\text{TiO}_2$  were also characterized by transient infrared absorption-excitation energy scanning spectroscopy (TRIRA-EESS), which can identify deep trapped electron energy levels above the valence band (VB) but below the Fermi level of the trapped electrons. Briefly, a 355 nm laser pulses from a Nd:YAG laser (Quanta Ray, Spectra Physics) with a pulse duration of 10 ns and a repetition rate of 10 Hz were used to pump an optical parametric oscillator (GWU premiScan-ULD/240, Spectra Physics) which acted as a wavelength-scanning excitation source (output signal beam tunable from 410 to 709 nm, and idler beam from 710 to 2630 nm) to excite the mid-gap states. The principle of TIRA-EESS is to scan the excitation energy within the band gap of  $\text{TiO}_2$  from the visible to near IR region, and use the transient mid-IR-difference spectra to probe the photo-excited electrons within the conduction band or

at the localized excited states below the CB. Both the CB electrons and the excited localized electrons can be detected by the mid-IR probe and distinguished by their remarkable difference in the corresponding absorption spectrum and the decay kinetics (slower decay for the former and faster decay for the latter). All the TIRA-EESS were probed at 2090  $\text{cm}^{-1}$  at a delay time of 250 ns after the excitation pulse in a chamber with a vacuum of  $1.0 \times 10^{-6}$  mbar. The excitation energy is 0.6 mJ/pulse with a beam size of 4 mm in diameter, and the IR absorbance has been scaled by the excitation intensity in terms of the number of photons ( $10^{12}$  per pulse).

### 2.3. Computational details

The calculation model of  $\text{TiO}_2$  is anatase phase. The calculated crystal structures are shown in Fig. S8. All the calculations were carried out using the density functional theory (DFT) based on the software package VASP. The exchange-correlation effects and core electrons were taken into account via the generalized gradient approximation (GGA-PBE). We considered Mg/Ni doping effects using  $2 \times 2 \times 2$  supercell. One Mg/Ni atom was filled in the interstitial position of  $\text{TiO}_2$ . The oxygen vacancy was next to the dopant. All the plane waves kinetic energy cut-off were set to 340 eV. The mechanical equilibrium was accomplished by conjugate gradient minimization of the forces to a tolerance of  $5 \times 10^{-2} \text{ eV}\text{\AA}^{-1}$ , and the atomic positions to a tolerance of  $2 \times 10^{-3} \text{ \AA}$ , the total energy to a tolerance of  $2 \times 10^{-6} \text{ eV}$ .

### 2.4. Photocatalytic reactions

Photocatalytic reactions were studied on Labsolar-III AG system. The samples were carried out in a Pyrex reaction vessel connected to a gas circulation system at room temperature. POWS was investigated in 100 mL of pure water containing 20 mg of samples. The light source was a 300-W xenon lamp (PLS-SXE300UV) and used the band filters to simulate it as AM 1.5 G sunlight. The reaction started without mechanical stirring and the solution was maintained at 5 °C by a water bath system. The evolved gases were analyzed by gas chromatography (TCD). Argon gas was used as the carrier gas.

### 2.5. Quantum efficiency (QE)

To obtain an accurate QE value, 100 mg sample was used in this measurement. And the experiment condition is similar to the POWS test. The quantum efficiency was calculated by the following equation:  $\Phi (\%) = (2 \times R/I) \times 100$ , where  $R$  and  $I$  represent the number of evolved  $\text{H}_2$  molecules and the number of absorbed photons in 1 h, respectively. Here,  $\Phi$  is the quantum efficiency. The light source was a 300-W xenon lamp attached with a band pass filter ( $\lambda = 350 \pm 10, 375 \pm 5, 400 \pm 5 \text{ nm}$ ). The intensity of the light irradiation was measured by a thermopile, which was located at the bottom of the reaction cell. For example, taking the measurement of QE for overall water splitting at 350 nm irradiation as a typical case, the irradiation intensity measured was  $0.31 \text{ mW/cm}^2$ . It corresponded to a total absorbed light energy in one hour of  $27.96 \text{ J}$ . We further took the average energy of photons at 350 nm to be 3.54 eV. The number of the absorbed photons would be  $4.92 \times 10^{19} \text{ h}^{-1}$ , which was considered as the  $I$  value. For the best samples, the rate of  $\text{H}_2$  evolution was  $7.94 \mu\text{mol h}^{-1}$ . Therefore, the total number of evolved  $\text{H}_2$  molecules in 1 h was  $4.78 \times 10^{18}$  ( $R$ ), and the calculated  $\Phi$  was 19.4% accordingly.

## 3. Results and discussions

In this work, the alkaline-earth metal Mg element was chosen to modify the property of anatase  $\text{TiO}_2$  nanostructures. Since

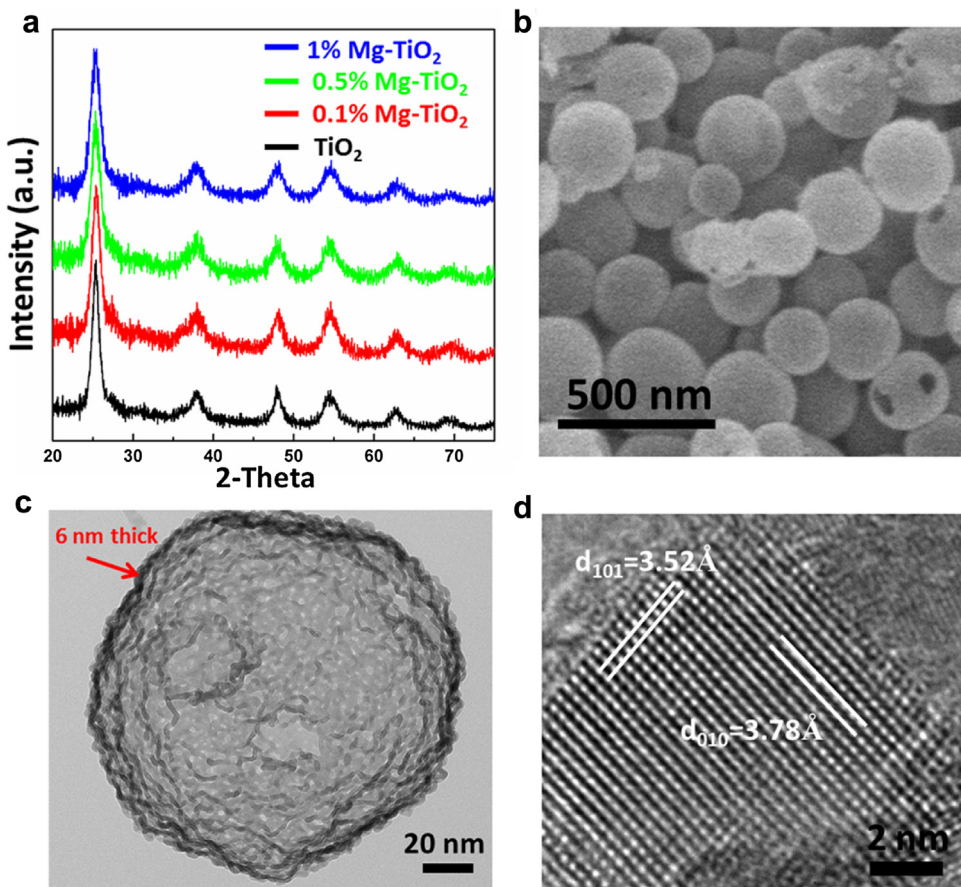


**Fig. 1.** (a) The XRD patterns of Mg-TiO<sub>2</sub> hollow sphere with 0, 0.1, 0.5, 1% Mg concentration, respectively. (b), (c) and (d) The SEM image, TEM image and HRTEM image of 0.5% Mg-TiO<sub>2</sub> hollow spheres.

the chemical activity of Mg and Ti elements is extremely different from each other, the uniform Mg doped anatase TiO<sub>2</sub> is hardly seen in previous reports [33]. Our Mg-doped TiO<sub>2</sub> (Mg-TiO<sub>2</sub>) ultrathin hollow spheres were synthesized by ions adsorption and templating method (Fig. S1) [34]. Inductive coupled plasma and atomic absorption spectroscopy (ICP-AAS) measurements reveals that the Mg contents in Mg-TiO<sub>2</sub> samples are varied from 0, 0.1, 0.5 to 1% (Mg/(Mg+Ti)) gradually with increasing the Mg content in adsorbed solution. Corresponding X-ray diffraction (XRD) patterns show that all the peaks of those samples are only assigned to anatase TiO<sub>2</sub> phase (Fig. 1a). Fig. S2 is the elements mapping of Mg-TiO<sub>2</sub> sample with high content of Mg, which shows an uniform distribution of Mg and Ti elements throughout the Mg-TiO<sub>2</sub> sample. X-ray photoelectron spectroscopy (XPS) illustrates that the valence state of Mg in Mg-TiO<sub>2</sub> is maintained as +2 value (Fig. S3) [35]. Scanning electron microscopy (SEM) image of 0.5% Mg-TiO<sub>2</sub> sample is shown in Fig. 1b. The 0.5% Mg-TiO<sub>2</sub> sample is grown in hollow sphere morphology with diameter about 200 nm. Fig. S4 illustrates that the other Mg-TiO<sub>2</sub> samples are also in similar hollow sphere morphology too. A transmission electron microscopy (TEM) image of 0.5% Mg-TiO<sub>2</sub> hollow sphere confirms that the shell of hollow sphere is 6 nm thick (Fig. 1c) and the specific surface area is at a level of 300 m<sup>2</sup> g<sup>-1</sup> (Fig. S5). Examination of the 0.5% Mg-TiO<sub>2</sub> with high-resolution (HR)-TEM shows that the lattice fringes are perpendicular interplanar spacings with  $d_{101} = 3.52 \text{ \AA}$  and  $d_{010} = 3.78 \text{ \AA}$ , which is consistent with the anatase crystal structure (Fig. 1d) [8].

To identify the Mg distribution in Mg-TiO<sub>2</sub> hollow spheres, the Raman spectra of pure TiO<sub>2</sub> and Mg-TiO<sub>2</sub> samples are shown in Fig. 2. As a powerful spectroscopic tool, Raman analysis is sensitive to the second phases and clusters of heterogeneous elements in

matrix. The bands appeared at 144 (Eg), 399 (B1g), 516 (A1g+B1g), and 639 cm<sup>-1</sup> (Eg) are the characteristic bands for anatase TiO<sub>2</sub> [36]. Furthermore, the positions of Raman bands for all Mg-TiO<sub>2</sub> hollow spheres are almost same to the bands observed in anatase TiO<sub>2</sub> (Fig. 2a), and, there are no redundant bands existed in the Raman spectra of Mg-TiO<sub>2</sub> hollow spheres. The result reveals that all the Mg-TiO<sub>2</sub> samples are pure anatase TiO<sub>2</sub> phase rather than containing Mg accumulated phases or clusters. The Mg substitution of Ti in TiO<sub>2</sub> would cause the distortion of TiO<sub>2</sub> Raman signals [37]. Therefore, the broadening and small shifts of Raman bands prove that the Mg ions in all Mg-TiO<sub>2</sub> samples are homogeneous doped in TiO<sub>2</sub> lattice (Fig. 2a and b). Those results confirm that the as-obtained samples are uniform Mg doped anatase TiO<sub>2</sub> ultrathin hollow spheres.

The ultraviolet-visible (UV-vis) absorption spectra of these as-prepared Mg-TiO<sub>2</sub> hollow spheres are presented in Fig. 3. It can be seen that the absorption edge shifts to blue side from 387 nm (3.2 eV) to 375 nm (3.30 eV) with increasing the Mg doping content. With increasing of the Mg dopants in low level (the highest Mg doping concentration is 1%), the band edge of Mg-TiO<sub>2</sub> is shifted only in 0.1 eV level. Therefore, the small amount of Mg doping can not change the band gap of TiO<sub>2</sub> drastically. Shown in the marked circle of Fig. 3, a clear band tailing in the range of 400–550 nm is detected from the pure anatase TiO<sub>2</sub> hollow spheres. Since the electrons transition from defect states are always resulted in light absorption, the intensity of band tailing could directly reflect the numbers of defect states. Thus, the clear band tailing illustrates the huge numbers of defects occurred on the ultrafine anatase TiO<sub>2</sub> nanostructures. Moreover, UV results show that the band tailing becomes weak after Mg doping and reduces to a minimum when

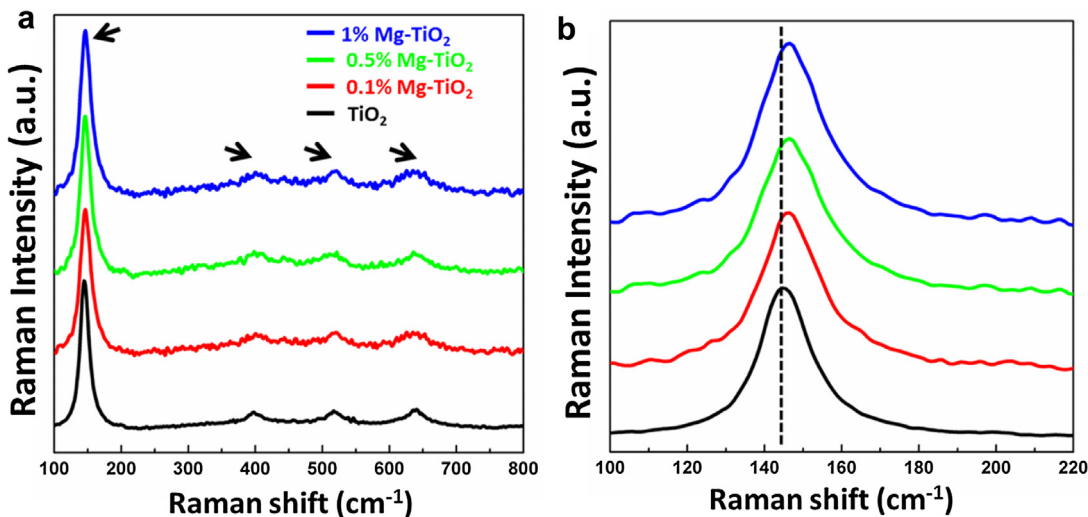


Fig. 2. (a) The Raman spectra of the pure and Mg-TiO<sub>2</sub> hollow spheres, respectively. (b) The fine Raman spectra between 100 and 220 cm<sup>-1</sup>.

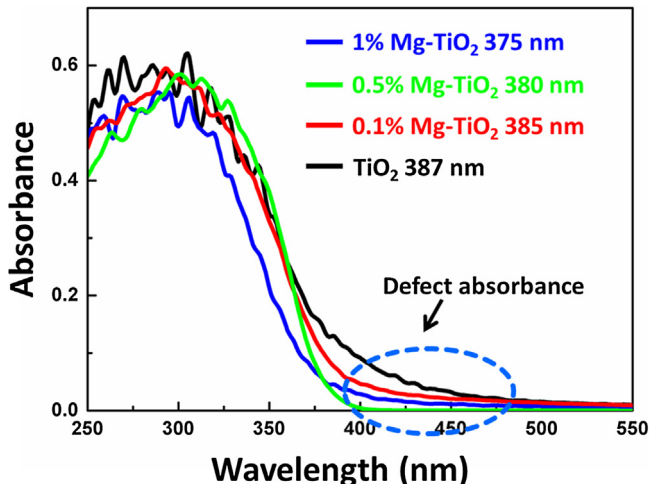


Fig. 3. UV-vis absorbance spectra of Mg-TiO<sub>2</sub> hollow sphere with 0, 0.1, 0.5, 1% Mg doping concentration, respectively. The curves are derived from diffuse reflectance data. (For interpretation of the references to colour in the text, the reader is referred to the web version of this article.)”.

the Mg doping at 0.5% level. It reveals that the Mg doping has the potential on weakening the defect states in anatase TiO<sub>2</sub>.

Interband defects are the main obstacle for POWS realization in anatase TiO<sub>2</sub>. The interband defect states change of TiO<sub>2</sub> after Mg doping was further characterized by transient infrared absorption-excitation energy scanning spectroscopy (TRIRA-EESS). The TRIRA-EESS shown in Fig. 4a report two different kinds of defect states: the deep defect states (occupied by electrons) higher than the valence band maximum (VBM) within the marked box and the shallow defect states (unoccupied) below the conduction band minimum (CBM). The energy position of deep defect states in pure anatase TiO<sub>2</sub> nanoparticles is near the VBM [19]. Fig. 4b shows the Schematic diagram of band structure of anatase TiO<sub>2</sub> hollow spheres before and after doped with Mg. The energy position of deep defect states in pure anatase TiO<sub>2</sub> nanoparticles could reduce the photocatalytic oxygen generated potential, thus, the pure anatase TiO<sub>2</sub> can not be used for POWS. After Mg doping, Fig. 4a shows that the deep defect states in anatase TiO<sub>2</sub> are eliminated throughly. The shallow defect states are also reduced with Mg doping and the density of shallow defect states reaches to the minimum when the Mg doping concentration is 0.5%. The density of

shallow defect states in 0.5% Mg-TiO<sub>2</sub> is only 1/3 of the pure anatase TiO<sub>2</sub> nanoparticles and pure rutile TiO<sub>2</sub> respectively (Fig. 4a and the rutile phase shown in Fig. S6). As schematic shown in Fig. 4b, the Mg doping could not only eliminate the deep defect states but also might significantly weaken the shallow defect states in TiO<sub>2</sub>. Thus, the photocatalytic reaction capacity of photo-generated electrons and holes are all strengthened by Mg doping, which provides the possibility for efficient sunlight-driven-POWS.

POWS performance of the Pt/Mg-TiO<sub>2</sub> ultrathin hollow spheres was tested under AM 1.5 G irradiation. No hydrogen was detected on the Pt/TiO<sub>2</sub> ultrathin hollow spheres. It confirmed that the pure TiO<sub>2</sub> ultrathin hollow spheres could not be used for POWS. After Mg doping, both H<sub>2</sub> and O<sub>2</sub> were produced simultaneously through the samples. Fig. 5a shows a typical time course for POWS on the impregnated Pt/0.5% Mg-TiO<sub>2</sub> under AM 1.5 G irradiation. Stoichiometric evolution of hydrogen and oxygen is evident from the start of the reaction, and there is even no clear degradation of gases generation in continuous 30 h test, which shows the excellent POWS stability. Pt/0.5% Mg-TiO<sub>2</sub> has the highest H<sub>2</sub> and O<sub>2</sub> evolution rates of 850 and 425  $\mu\text{mol g}^{-1} \text{h}^{-1}$ , respectively (Fig. 5b) and generated bubbles can be seen in the POWS test (Supplementary Movie S1, see Supporting information). We calculated the POWS apparent quantum efficiency (QE) of the 0.5% Mg-TiO<sub>2</sub> hollow spheres under different wavelength. The estimated QE is 0%, 4.2%, 19.4% under 400, 375, 350 nm wavelength respectively. Therefore, the efficient and stable sunlight-driven-POWS is realized on anatase TiO<sub>2</sub> hollow spheres for the first time with Mg doping. Additionally, the performance of POWS exhibits a bell-shaped change with increasing of the Mg content, which is proportional to the density of defect states in Mg-TiO<sub>2</sub> samples (Fig. 5b).

Introducing heterogeneous elements in TiO<sub>2</sub> have been shown to produce more defect states [38,39]. We also synthesized the TiO<sub>2</sub> hollow spheres doped with Ni, Cr elements. And, there is no POWS signal detected on those samples. Fig. 6a shows the total density of states (TDOS) of pure TiO<sub>2</sub> and Mg, Ni doped TiO<sub>2</sub> (crystal structure shown in Fig. S7). It reveals that no defect states are occurred in the band gap of those samples except of the Ni doped TiO<sub>2</sub>. The new defect states in Ni doped TiO<sub>2</sub> have been confirmed that was introduced by the d orbit of Ni dopants [40]. And it is also evident by the partial DOS calculation shown in Fig. 6c. Since Mg atoms have no d orbit, the Mg doping would not generate new defect states in TiO<sub>2</sub>. However, TiO<sub>2</sub> have many intrinsic defects, such as oxygen vacancy (V<sub>O</sub>), could introduce defect states too. Fig. 6b illustrates that V<sub>O</sub> states in TiO<sub>2</sub> are located in the band gap. Interestingly,

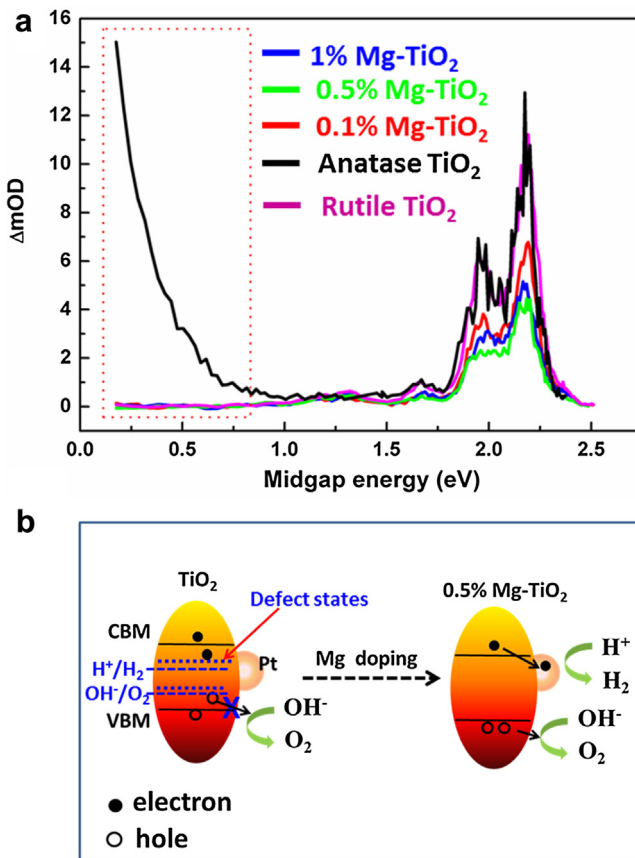


**Fig. 4.** (a) Transient IR absorption–excitation energy scanning spectra for 0.1, 0.5, 1% Mg-TiO<sub>2</sub> hollow spheres, pure anatase and rutile TiO<sub>2</sub>. (b) Schematic evolution of the trapping states and the water splitting reactions of anatase TiO<sub>2</sub> before and after Mg doping.

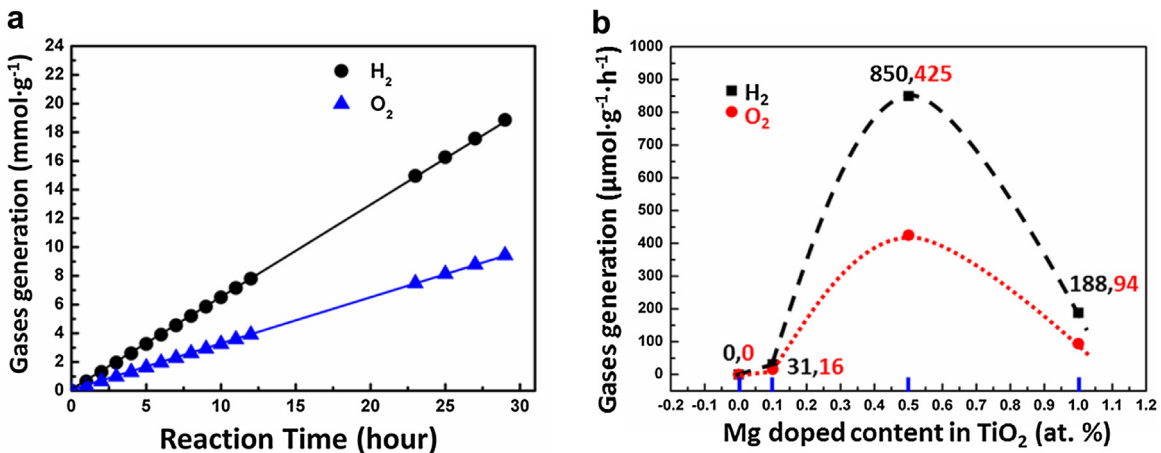


**Fig. 5.** (a) Time course of POWS on the 0.5% Mg-TiO<sub>2</sub> hollow spheres decorated with Pt. (b) POWS gases generation rates of Mg-TiO<sub>2</sub> hollow sphere with 0, 0.1, 0.5, 1% Mg doping concentration.

the states introduced by Vo are quenched and strengthened by Mg and Ni doping respectively. With introducing Vo in TiO<sub>2</sub> (TiO<sub>2</sub> + Vo), the 3d orbit of Ni dopant produces more defect states in band gap (Fig. 6c). It reveals that the 3d orbit of Ni could hybrid with the intrinsic defect states to cause more states in band gap. The DOS of Mg dopant is not distributed in the band gap of TiO<sub>2</sub> too with introduction of Vo (Fig. 6d). Moreover, the 2p orbit of Mg could also hybrid the intrinsic defect states in TiO<sub>2</sub> too. Since the 2p orbit of Mg is far away from the CBM and VBM of TiO<sub>2</sub> (Fig. 6d), the 2p orbit of Mg dopant could hybrid the intrinsic defect states in TiO<sub>2</sub> to change the energy level of the defect states to get them out of the

band gap, thereby eliminating the intrinsic defect states in anatase TiO<sub>2</sub>.

#### 4. Conclusions

In summary, a facile ions adsorption and templating method was used to synthesize the Mg doped anatase TiO<sub>2</sub> ultrathin hollow spheres, with a shell thickness of about 6 nm and a specific surface area about 300 m<sup>2</sup> g<sup>-1</sup>. XRD, EDS mapping and Raman test show the uniform Mg doping in our synthesized Mg-TiO<sub>2</sub> samples. Through the TRIRA-EESS measurement, it has been found

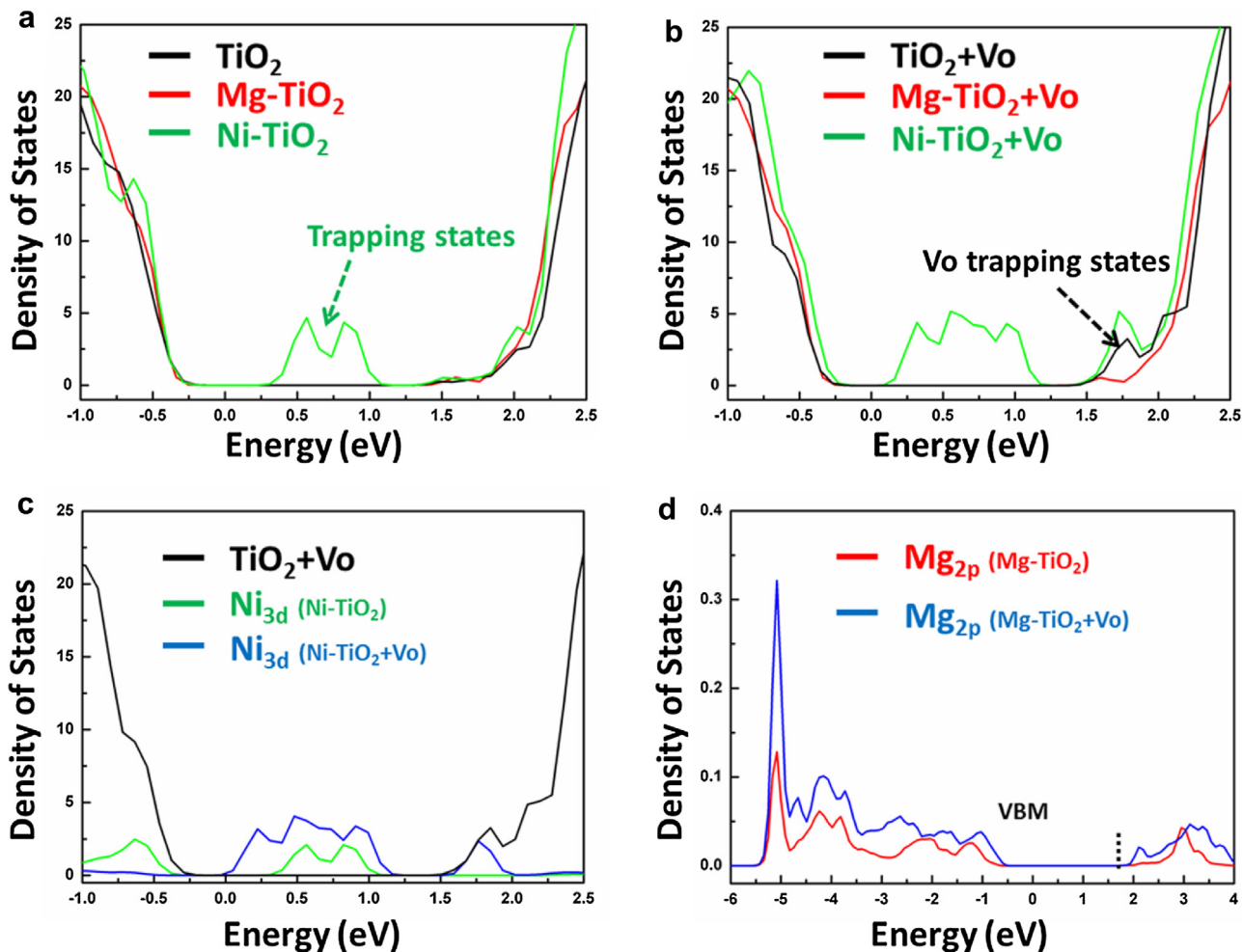


**Fig. 6.** (a) The calculated total density of state (TDOS) of pure  $\text{TiO}_2$ , Ni doped  $\text{TiO}_2$  and Mg doped  $\text{TiO}_2$ . (b) The TDOS of pure  $\text{TiO}_2$ , Ni doped  $\text{TiO}_2$  and Mg doped  $\text{TiO}_2$  with oxygen vacancy (Vo). (c) The calculated TDOS of  $\text{TiO}_2$  with Vo ( $\text{TiO}_2$  + Vo) and the DOS of 3d orbit of Ni dopant in  $\text{TiO}_2$  and  $\text{TiO}_2$  + Vo. (d) The DOS of 2p orbit of Mg dopant in  $\text{TiO}_2$  and  $\text{TiO}_2$  + Vo.

that the Mg dopants could eliminate the deep defect states near the VBM, thus, realizing the photocatalytic overall water splitting. Moreover, the Mg doping could reduce the shallow defect states under CBM in  $\text{TiO}_2$ , thereby further increasing the photocatalytic performance. First principle calculations reveal that the 2p orbit of Mg dopant could hybrid with the intrinsic defect states induced by oxygen vacancy and get those defect states out of the band gap. High efficient and stable photocatalytic overall water splitting is firstly occurred on the Pt decorated 0.5% Mg-TiO<sub>2</sub> ultrathin hollow spheres. The H<sub>2</sub> and O<sub>2</sub> evolution rates can be as high as 850 and 425  $\mu\text{mol g}^{-1} \text{h}^{-1}$  respectively under AM 1.5 G irradiation and the apparent quantum efficiency of 19.4% is achieved under 350 nm light irradiation.

## Acknowledgements

This work is supported by the Outstanding Youth Foundation of Hebei Province (Grant No. A2016201176), the National Nature Science Foundation of China (Grant No. 51372064) and the Outstanding Doctoral Cultivation Project of Hebei University (YB201502). Y. Hu acknowledges financial support from Zhejiang Provincial Natural Science Foundation of China (LR14B010001), the Zhejiang Provincial Public Welfare Project (2016C31015) and National Nature Science Foundation of China (Grant No. 21671173).

## Appendix A. Supplementary data

Supplementary data associated with this article can be found, in the online version, at <http://dx.doi.org/10.1016/j.apcatb.2016.09.018>.

## References

- [1] J. Liu, Y. Liu, N. Liu, Y. Han, X. Zhang, H. Huang, Y. Lifshitz, S.-T. Lee, J. Zhong, Z. Kang, Metal-free efficient photocatalyst for stable visible water splitting via a two-electron pathway, *Science* 347 (2015) 970–974.
- [2] A. Kudo, Y. Miseki, Heterogeneous photocatalyst materials for water splitting, *Chem. Soc. Rev.* 38 (2009) 253–278.
- [3] X. Li, J. Yu, J. Low, Y. Fang, J. Xiao, X. Chen, Engineering heterogeneous semiconductors for solar water splitting, *J. Mater. Chem. A* 3 (2015) 2485–2534.
- [4] X. Chen, L. Liu, F. Huang, Black titanium dioxide ( $\text{TiO}_2$ ) nanomaterials, *Chem. Soc. Rev.* 44 (2015) 1861–1885.
- [5] A. Kasahara, K. Nukumizu, G. Hitoki, T. Takata, J.N. Kondo, M. Hara, H. Kobayashi, K. Domen, Photoreactions on  $\text{LaTiO}_2\text{N}$  under visible light irradiation, *J. Phys. Chem. A* 106 (2002) 6750–6753.
- [6] R.D. Smith, M.S. Prevot, R.D. Fagan, Z. Zhang, P.A. Sedach, M.K. Siu, S. Trudel, C.P. Berlinguette, Photochemical route for accessing amorphous metal oxide materials for water oxidation catalysis, *Science* 340 (2013) 60–63.
- [7] Y. Ide, N. Inami, H. Hattori, K. Saito, M. Sohmiya, N. Tsunooji, K. Komaguchi, T. Sano, Y. Bando, D. Golberg, Y. Sugahara, Remarkable charge separation and photocatalytic efficiency enhancement through interconnection of  $\text{TiO}_2$  nanoparticles by hydrothermal treatment, *Angew. Chem. Int. Ed.* 55 (2016) 3600–3605.

[8] Y. Liu, B. Zhang, L. Luo, X. Chen, Z. Wang, E. Wu, D. Su, W. Huang, TiO<sub>2</sub>/Cu<sub>2</sub>O core/ultrathin shell nanorods as efficient and stable photocatalysts for water reduction, *Angew. Chem. Int. Ed.* 54 (2015) 15260–15265.

[9] E. Borgarello, J. Kiwi, M. Graetzel, E. Pelizzetti, M. Visca, Visible light induced water cleavage in colloidal solutions of chromium-doped titanium dioxide particles, *J. Am. Chem. Soc.* 104 (1982) 2996–3002.

[10] R. Asahi, T. Morikawa, T. Ohwaki, K. Aoki, Y. Taga, Visible-light photocatalysis in nitrogen-doped titanium oxides, *Science* 293 (2001) 269–271.

[11] H.-i. Kim, D. Monllor-Satoca, W. Kim, W. Choi, N-doped TiO<sub>2</sub> nanotubes coated with a thin TaO<sub>x</sub>N<sub>y</sub>layer for photoelectrochemical water splitting: dual bulk and surface modification of photoanodes, *Energy Environ. Sci.* 8 (2015) 247–257.

[12] L. Mao, Y. Wang, Y. Zhong, J. Ning, Y. Hu, Microwave-assisted deposition of metal sulfide/oxide nanocrystals onto a 3D hierarchical flower-like TiO<sub>2</sub> nanostructure with improved photocatalytic activity, *J. Mater. Chem. A* 1 (2013) 8101–8104.

[13] J. Wang, A. Ma, Z. Li, J. Jiang, J. Feng, Z. Zou, Unraveling the mechanism of 720 nm sub-band-gap optical absorption of a Ta<sub>3</sub>N<sub>5</sub> semiconductor photocatalyst: a hybrid-DFT calculation, *Phys. Chem. Chem. Phys. PCCP* 17 (2015) 8166–8171.

[14] A. Naldoni, M. Allieta, S. Santangelo, M. Marelli, F. Fabbri, S. Cappelli, C.L. Bianchi, R. Psaro, V. Dal Santo, Effect of nature and location of defects on bandgap narrowing in black TiO<sub>2</sub> nanoparticles, *J. Am. Chem. Soc.* 134 (2012) 7600–7603.

[15] G. Liu, L.-C. Yin, J. Wang, P. Niu, C. Zhen, Y. Xie, H.-M. Cheng, A red anatase TiO<sub>2</sub> photocatalyst for solar energy conversion, *Energy Environ. Sci.* 5 (2012) 9603.

[16] Y. Li, L. Zhu, Y. Guo, H. Song, Z. Lou, Z. Ye, A new type of hybrid nanostructure: complete photo-generated carrier separation and ultrahigh photocatalytic activity, *J. Mater. Chem. A* 2 (2014) 14245–14250.

[17] H. Tong, S. Ouyang, Y. Bi, N. Umezawa, M. Oshikiri, J. Ye, Nano-photocatalytic materials: possibilities and challenges, *Adv. Mater.* 24 (2012) 229–251.

[18] M. Zhu, Y. Mi, G. Zhu, D. Li, Y. Wang, Y. Weng, Determination of midgap state energy levels of an anatase TiO<sub>2</sub> nanocrystal film by nanosecond transient infrared absorption –excitation energy scanning spectra, *J. Phys. Chem. C* 117 (2013) 18863–18869.

[19] R. Li, Y. Weng, X. Zhou, X. Wang, Y. Mi, R. Chong, H. Han, C. Li, Achieving overall water splitting using titanium dioxide-based photocatalysts of different phases, *Energy Environ. Sci.* 8 (2015) 2377–2382.

[20] D.V. Bavykin, J.M. Friedrich, F.C. Walsh, Protonated titanates and TiO<sub>2</sub> nanostructured materials: synthesis, properties, and applications, *Adv. Mater.* 18 (2006) 2807–2824.

[21] I.-S. Park, S.-R. Jang, J.S. Hong, R. Vittal, K.-J. Kim, Preparation of composite anatase TiO<sub>2</sub> nanostructure by precipitation from hydrolyzed TiCl<sub>4</sub> solution using anodic alumina membrane, *Chem. Mater.* 15 (2003) 4633–4636.

[22] X. Li, J. Yu, M. Jaroniec, Hierarchical photocatalysts, *Chem. Soc. Rev.* 45 (2016) 2603–2636.

[23] R.T. Ako, P. Ekanayake, D.J. Young, J. Hobley, V. Chellappan, A.L. Tan, S. Gorelik, G.S. Subramanian, C.M. Lim, Evaluation of surface energy state distribution and bulk defect concentration in DSSC photoanodes based on Sn, Fe, and Cu doped TiO<sub>2</sub>, *Appl. Surf. Sci.* 351 (2015) 950–961.

[24] D. Lu, B. Zhao, P. Fang, S. Zhai, D. Li, Z. Chen, W. Wu, W. Chai, Y. Wu, N. Qi, Facile one-pot fabrication and high photocatalytic performance of vanadium doped TiO<sub>2</sub>-based nanosheets for visible-light-driven degradation of RhB or Cr(VI), *Appl. Surf. Sci.* 359 (2015) 435–448.

[25] Z. Sayyar, A. Akbar Babalou, J.R. Shahrouzi, Kinetic study of formic acid degradation by Fe<sup>3+</sup> doped TiO<sub>2</sub> self-cleaning nanostructure surfaces prepared by cold spray, *Appl. Surf. Sci.* 335 (2015) 1–10.

[26] M. Wen, S. Zhang, W. Dai, G. Li, D. Zhang, In situ synthesis of Ti<sup>3+</sup> self-doped mesoporous TiO<sub>2</sub> as a durable photocatalyst for environmental remediation, *Chin. J. Catal.* 36 (2015) 2095–2102.

[27] J. Wen, X. Li, W. Liu, Y. Fang, J. Xie, Y. Xu, Photocatalysis fundamentals and surface modification of TiO<sub>2</sub> nanomaterials, *Chin. J. Catal.* 36 (2015) 2049–2070.

[28] S. Iwamoto, Y. Sazanami, M. Inoue, T. Inoue, T. Hoshi, K. Shigaki, M. Kaneko, A. Maenosono, Fabrication of dye-sensitized solar cells with an open-circuit photovoltage of 1 V, *Chem. Sustain. Chem.* 1 (2008) 401–403.

[29] K. Kakiage, T. Tokutome, S. Iwamoto, T. Kyomen, M. Hanaya, Fabrication of a dye-sensitized solar cell containing a Mg-doped TiO<sub>2</sub> electrode and a Br<sup>3-</sup>/Br<sup>-</sup> redox mediator with a high open-circuit photovoltage of 1.21 V, *Chem. Commun.* 49 (2013) 179–180.

[30] X. Sun, Y. Li, Colloidal carbon spheres and their core/shell structures with noble-metal nanoparticles, *Angew. Chem. Int. Ed.* 43 (2004) 597–601.

[31] X. Sun, J. Liu, Y. Li, Use of carbonaceous polysaccharide microspheres as templates for fabricating metal oxide hollow spheres, *Chem.–A Eur. J.* 12 (2006) 2039–2047.

[32] Y. Li, X. Cheng, X. Ruan, H. Song, Z. Lou, Z. Ye, L. Zhu, Enhancing photocatalytic activity for visible-light-driven H<sub>2</sub> generation with the surface reconstructed LaTiO<sub>2</sub>N nanostructures, *Nano Energy* 12 (2015) 775–784.

[33] Z. Wu, Y. Li, L. Gao, S. Wang, G. Fu, Synthesis of Na-doped ZnO hollow spheres with improved photocatalytic activity for hydrogen production, *Dalton Trans.* 45 (2016).

[34] M. Xiao, Y. Li, Y. Lu, Z. Ye, Synthesis of ZrO<sub>2</sub>:Fe nanostructures with visible-light driven H<sub>2</sub> evolution activity, *J. Mater. Chem. A* 3 (2015) 2701–2706.

[35] J. Seo, T. Takata, M. Nakabayashi, T. Hisatomi, N. Shibata, T. Minegishi, K. Domen, Mg-Zr cosubstituted Ta<sub>3</sub>N<sub>5</sub> photoanode for lower-onset-potential solar-driven photoelectrochemical water splitting, *J. Am. Chem. Soc.* 137 (2015) 12780–12783.

[36] X. Zong, Z. Xing, H. Yu, Z. Chen, F. Tang, J. Zou, G.Q. Lu, L. Wang, Photocatalytic water oxidation on F, N co-doped TiO<sub>2</sub> with dominant exposed {001} facets under visible light, *Chem. Commun.* 47 (2011) 11742–11744.

[37] M. Xu, T. Liang, M. Shi, H. Chen, Graphene-like two-dimensional materials, *Chem. Rev.* 113 (2013) 3766–3798.

[38] X. Zhou, V. Häublein, N. Liu, N.T. Nguyen, E.M. Zolnhofer, H. Tsuchiya, M.S. Killian, K. Meyer, L. Frey, P. Schmuki, TiO<sub>2</sub> nanotubes: nitrogen-ion implantation at low dose provides noble-metal-free photocatalytic H<sub>2</sub>-evolution activity, *Angew. Chem. Int. Ed.* 55 (2016) 3763–3767.

[39] Z. Yao, F. Jia, S. Tian, C. Li, Z. Jiang, X. Bai, Microporous Ni-doped TiO<sub>2</sub> film photocatalyst by plasma electrolytic oxidation, *ACS Appl. Mater. Interfaces* 2 (2010) 2617–2622.

[40] M.S. Park, S.K. Kwon, B.I. Min, Electronic structures of doped anatase TiO<sub>2</sub>: Ti<sub>1-x</sub>M<sub>x</sub>O<sub>2</sub> (M = Co, Mn, Fe, Ni), *Phys. Rev. B* 65 (2002) 161201.